proceedings

MDPI

Proceedings

Understanding the Aerodynamic Benefits of Drafting in the Wake of Cyclists †

Christopher Brown *, Timothy Crouch, David Burton and Mark C. Thompson

Mechanical and Aerospace Engineering, Monash University, Clayton 3800, Australia; timothy.crouch@monash.edu (T.C.); david.burton@monash.edu (D.B.); mark.thompson@monash.edu (M.C.T.)

* Correspondence: Christopher.brown@monash.edu; Tel.: +61-(0)4-11-872-497

† Presented at the 13th conference of the International Sports Engineering Association, Online, 22–26 June 2020.

Published: 15 June 2020

Abstract: A new approach is presented to characterize the aerodynamic benefit from riding in the wake of another cyclist at different downstream locations. The method presented uses the dynamic pressure deficit in the wake of a cycling mannequin to estimate percentage drag savings. In the experiments, the time-averaged velocity behind a cycling mannequin was recorded in 1 × 0.95 m cross-planes by two four-hole pressure (Cobra) probes for four static leg positions (0°, 90°, 180°, and 270°). It was found that the wake of the cycling mannequin propagated to one side or the other as it developed downstream, depending on the strength of the two large-scale counter-rotating streamwise vortical structures shed off the hips of the mannequin. In the near wake, the complex wake dynamics resulted in an inaccurate prediction of the relative drag reduction based upon a dynamic pressure deficit. However, as the wake developed and stabilised further downstream, the dynamic pressure deficit was found to provide a reasonable estimate of the aerodynamic drag reduction of riding in the wake of the lead rider.

Keywords: cycling aerodynamics; wake dynamics; speed sports; aerodynamic drag

1. Introduction

Cycling aerodynamics is a unique sub-class of bluff-body aerodynamics. The dynamic leg motion during the pedal stroke provides a complex three-dimensional flow field in the wake of a cyclist. As flow separates from the body of a cyclist, a large velocity deficit and energy loss occurs as vortical flow structures are generated in the wake. The shape of an athlete is far from optimal aerodynamically, and both academic literature and industry have developed methods to assess and reduce the aerodynamic drag. Almost all studies, both numerical and experimental, have conducted their research within an environment with little to no oncoming turbulence present. In addition, when competing on a velodrome, an athlete rides in the near or far wake of teammates or competitors. A number of different academic groups have conducted research on the near-wake interaction between riders in team-pursuit configurations [1–3]. However, to the best of the authors' knowledge, limited research has been conducted on how a wake of a single cyclist develops in the far field and the aerodynamic benefits from riding in these far field wakes. This research begins to explore the complexity of the far-field wake behind a cyclist and the effects on trailing riders.

Measurements were taken simultaneously with two four-hole probes mounted on a two-axis traverse at various downstream locations behind a static-leg mannequin. In contrast to using direct drag measurements, the approach presented in this paper uses the reduction of dynamic pressure as a function of downstream distance to estimate an aerodynamic drag savings when compared to a solo rider. Beyond this, the paper aims to provide some understanding of how the wake develops as

it advects downstream, and discusses the benefits from riding in the far field wake of upstream cyclists.

2. Methodology

Aerodynamic drag savings from riding in the wakes of competitors has been explored by direct drag measurements at different axial separations [2,4,5], although mostly focusing on relatively small separations. As a cyclist is a form of bluff body, the dominant aerodynamic force is pressure drag [6]. Using planes of dynamic pressure in the wake of a mannequin holding static leg positions, an average dynamic pressure across the frontal area of a trailing rider is given by:

$$\bar{Q}_{wake} = \frac{\iint \frac{1}{2}\rho \bar{u}(y,z)^2 dA}{A}, \quad (1)$$

where $\bar{Q}_{wake}$ = average dynamic pressure acting across the projected area, ρ = air density, $\bar{u}(y,z)$ = time-mean streamwise velocity, and A = projected frontal area of the trailing riding. The integration area, A, used for this experiment is based upon the static leg mannequin in the 0° leg position. The integration area of the Monash cyclist mannequin was 0.28 m^2.

The difference in mean dynamic pressure experienced between a solo rider and the calculated dynamic pressure of a rider in the wake, can be used to provide an estimate of the drag reduction from riding in the wake of another cyclist, i.e.,

$$Drag(\%) = \left[\frac{Q_\infty - \bar{Q}_{wake}}{Q_\infty}\right] \times 100, \quad (2)$$

where *Drag* (%) = percentage drag reduction and Q_∞ = average freestream dynamic pressure. Based upon the aerodynamic drag of a cyclist being dominated by pressure drag, Equation (2) approximates the aerodynamic savings available when riding in the wake of another cyclist.

3. Experimental Setup and Procedures

Experimental Setup

The experiments were conducted in the Monash Large Wind Tunnel of the FLAIR (Fluids Laboratory for Aeronautical and Industrial Research) group at Monash University. The wind tunnel has a cross section of 4 × 2.6 m with a turbulence intensity of 1.5% at the selected measurement wind speed. Tests were conducted at 16 m/s, a representative speed of an elite male endurance athlete. The Monash cycling mannequin in the time trial position was used across all tests. The mannequin was on board a standard endurance size 54 frame with two Mavic wheels held by two supports (Figure 1). Experiments were conducted with the mannequin in four leg positions; two low-drag positions (0° and 180°) and two high drag positions (90° and 270°) [7]. Here, 0° corresponds to the crank horizontal with the right leg forward.

Wake velocities were recorded by two 4-hole pressure probes (Cobra probes) connected to a two-axis traverse system (Figure 1). The 4-hole pressure probes sampled at 2000 Hz for 10.1 s and are separated by 0.1 m on the two-axis traverse system. Measurements were taken across a cross-sectional area of 0.95 m^2 with 0.05 m spacing in Y and Z. Table 1 outlines the details of the traverse measurement locations and limits across all tests. Streamwise measurement locations chosen were based upon the torso length of 0.63 m of the Monash cycling mannequin.

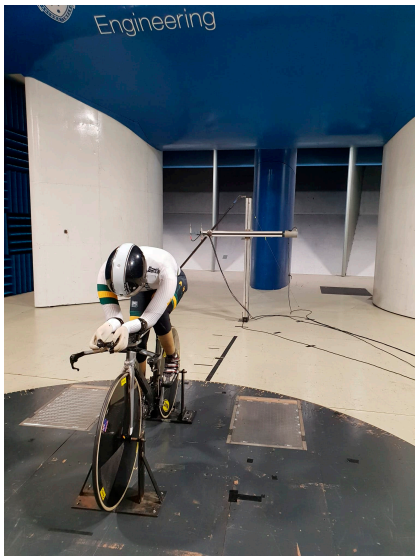

Figure 1. Wind-tunnel set up of the Monash cycling mannequin and probe measurement system in the wake.

Table 1. Measurement details of the two dynamic pressure probes in the wake of the Monash cycling mannequin.

Leg Position	*X* Location (m)	Y Limits(m)	Z Limits (m)
0°	0.63, 1.26, 2.52, 3.78, 5.04, 6.93	[−0.50 0.50]	[0.45 1.40]
90°	0.63, 1.26, 2.52, 3.78, 5.04	[−0.50 0.50]	[0.45 1.40]
180°	1.26,2.52	[−0.50 0.50]	[0.45 1.40]
270°	1.26,2.52	[−0.50 0.50]	[0.45 1.40]

4. Results

4.1. Wake Development

Unsurprisingly, the time-averaged velocity field in the wake of the mannequin changes significantly as the fluid propagates downstream. Figure 2 shows the non-dimensional time-average streamwise velocity contours overlaid with in-plane velocity vectors at 6 cross-planes downstream of the mannequin. These images show results for the 0° low-drag leg position. It is observed that, as the wake travels downstream, the position of maximum velocity deficit moves laterally, both to the right side and towards the ground. The asymmetry of the leg position produces an uneven fluid forcing and causes rotation of fluid in the wake, with the latter dominated by the two large-scale streamwise vortical structures shed from either hip [7]. At the closest measurement location, shown in Figure 2a, the right hip vortex has a more significant rotation with almost double the magnitude of circulation.

Measurements indicate that the development of the wake as it propagates downstream is consistent across four leg positions (0°, 90°, 180°, and 270°). Figure 3 displays contour maps of the streamwise velocity at 2.52 m behind the mannequin for all four leg positions. Figure 3a,b shows a stronger vortex shed off the right hip whilst Figure 3c,d shows the reverse [8]. It is evident that there is a trend for the wake to propagate towards the stronger vortex of the counter-rotating streamwise pair shed from the mannequin. In the two low-drag positions (0° and 180°), the wake tends towards the side of the leg positioned further upstream in the high drag positions (90° and 270°), there is a large downwash and sideways propagation towards the outstretched leg. This sideways wake propagation towards the side of the outstretched leg continues as the wake develops downstream.

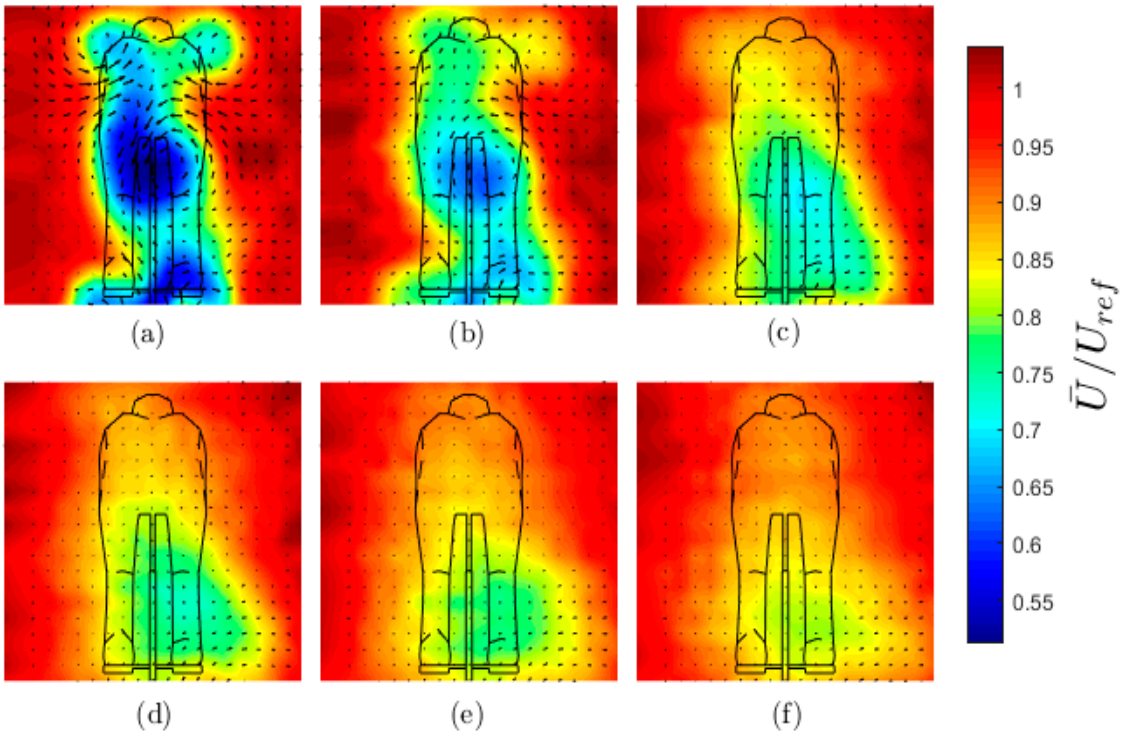

Figure 2. The time-average velocity color contour maps of the streamwise velocity (u) overlaid with projected velocity vectors in Y-Z planes behind the Monash cycling mannequin with the legs in the low drag (0°) position. Downstream locations are: (**a**) 0.63 m; (**b**) 1.26 m; (**c**) 2.52 m; (**d**) 3.78 m; (**e**) 5.04 m; and (**f**) 6.93 m.

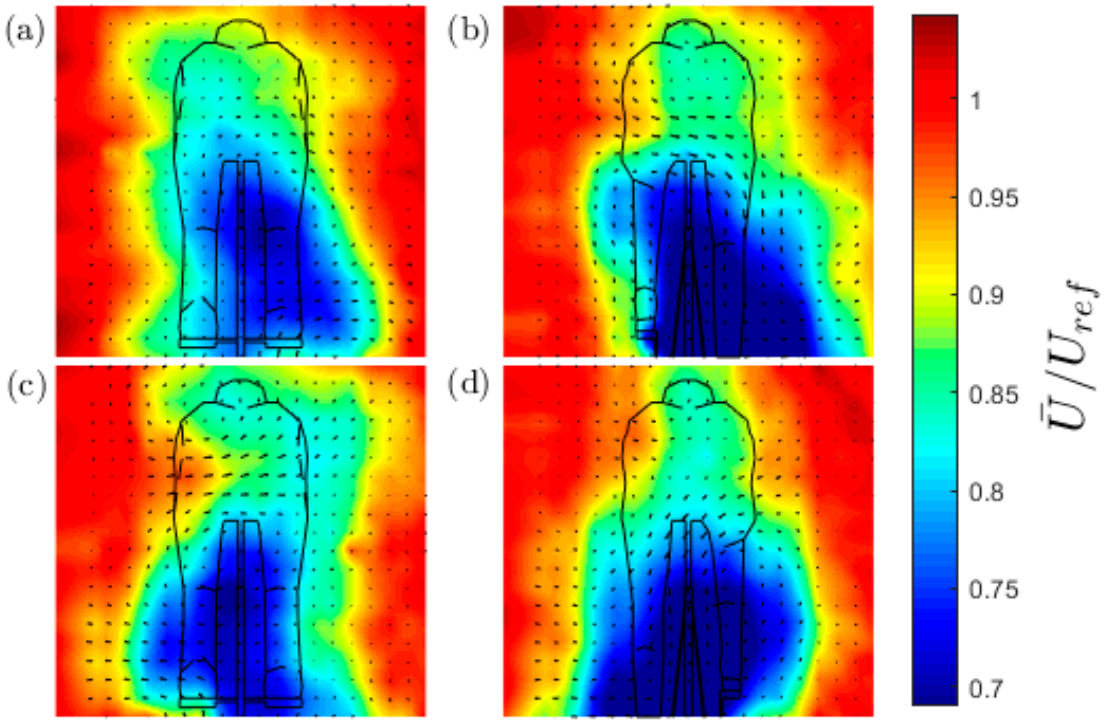

Figure 3. Time-average velocity color contour maps of the streamwise velocity (u) and overlaid velocity vectors in the Y-Z planes 2.52 m behind the mannequin in leg positions: (**a**) 0°; (**b**) 90°; (**c**) 180°; and (**d**) 270°.

4.2. Drag Reduction (%)

Deduced from Equation (2), the percentage drag reduction for a trailing cyclist at different downstream positions and for different leg positions is plotted in Figure 4. It is evident that this drag reduction estimate based upon dynamic pressure loss slightly overestimates the induced drag reduction when compared to the direct drag measurements of Barry [4], particularly in the near wake. There are probably a number of factors causing this over estimation. Amongst these is the assumption that mean dynamic pressure reduction over the cyclist's frontal area is directly related to drag, and that the flow past the trailing cyclist is effectively equivalent to that past the leading cyclist, so that the drag contributions of each body/cycle component remain the same. Related to this, certain components of an athlete and bike contribute more to the overall aerodynamic drag than others. Computational results presented by Griffith [9] highlight how the torso of the Monash cycling mannequin contributes more drag area (~22.5%) when compared to the right leg (~15%) or left leg (~11%) in the 0° leg position. Figure 5 highlights the two contour maps used to calculate the dynamic pressure loss at the closest location to the mannequin in the low and high drag leg position (0° & 90°). It is evident that there are large concentrated regions of low dynamic pressure over both legs and a high dynamic pressure region over the torso. This irregular distribution of dynamic pressure significantly affects the approximation and results in a higher estimate of the percentage drag reduction. Even in this case, the estimate is only about 20% too high.

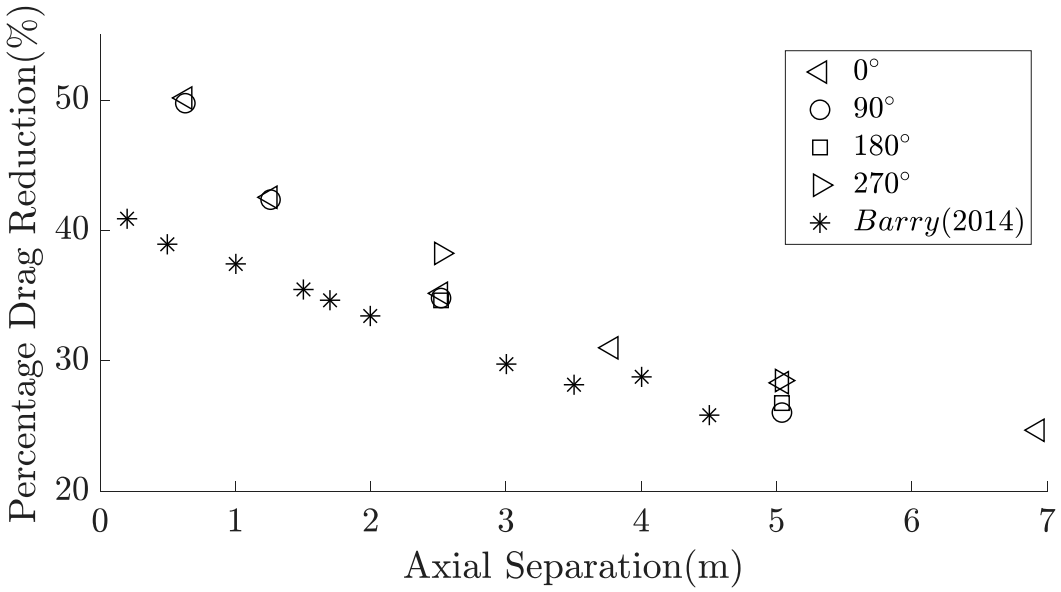

Figure 4. Percentage drag reduction (%) based upon the dynamic pressure difference for different axial separations of a trailing rider in the wake of the cycling mannequin for leg positions: 0°; 90°; 180°; 270°. The results obtained by Barry [4] are from direct force measurements of a trailing dynamic athlete in the wake of the Monash cycling mannequin with legs positioned at 15°.

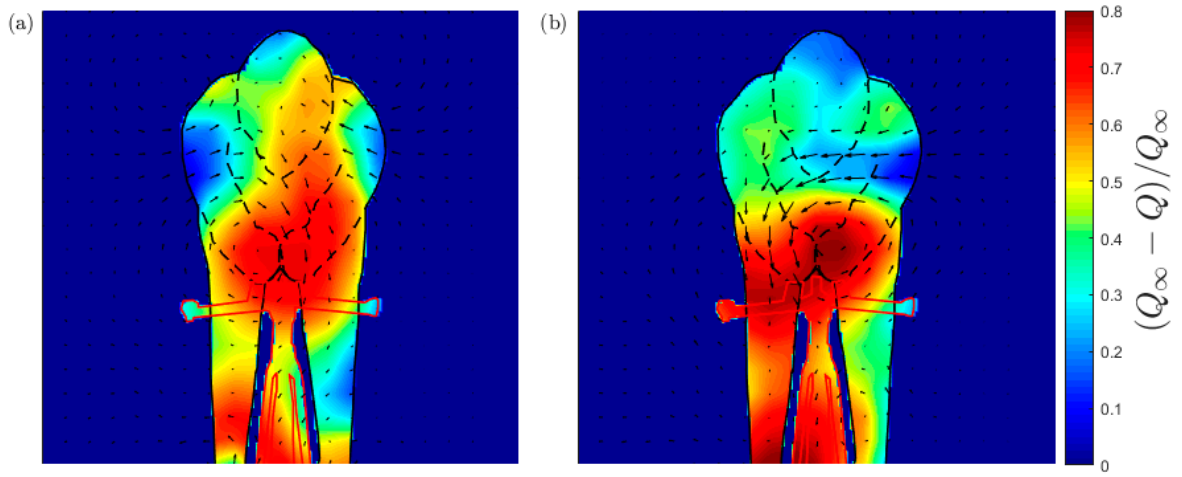

Figure 5. Front view of the integration area of the time-average dynamic pressure savings contour map of the streamwise velocity (u) in the Y-Z plane 0.63 m behind a static legged mannequin in the (**a**) 0° leg position; (**b**) 90° leg position.

As the wake develops downstream, the percentage drag reduction based upon the dynamic pressure loss approaches that found by direct drag measurements. As the large-scale vortical structures diffuse and mix laterally, the dynamic pressure distribution becomes more evenly distributed. This, in turn, allows for a more reliable estimate across the frontal area of a cyclist from this technique. Given this, it could be expected that even further downstream into the far wake of a pedaling athlete (>6 m), an average of the dynamic pressure deficit across multiple leg positions would predict the aerodynamic savings reasonably accurately. Furthermore, understanding how the distribution of dynamic pressure develops in the far wake (>10 m) would allow for the methods described herein to be extended to a wider range of cycling events. An understanding of the turbulent properties of the wake at these distances would also contribute significantly to optimising cycling aerodynamic performance for these turbulent flow fields. Turbulent flow fields are known to effect flow transition and separation phenomena from bluff body geometries [10] which are critical to the magnitude of the aerodynamic forces that a cyclist will experience.

5. Conclusions

Time-average velocity fields were measured in the wake of the Monash cycling mannequin across four different leg positions. As the wake develops into the far field, there is a clear dependence on the initial asymmetry in the flow field in the near wake, in turn caused by asymmetry of the cyclist. The difference in circulation between the large-scale structures combined with acceleration of fluid flow over elements of the cyclist geometry result in the wake tending towards one side. Due to this large asymmetry, the dynamic pressure deficit is not evenly distributed across the integration area and results in the estimated percentage drag savings to be overestimated. However, further downstream in the wake, as it reaches a more self-similar state and varies less across the cyclist's frontal area, the percentage drag saving based upon the mean dynamic pressure deficit provides a more accurate drag reduction estimate.

Conflicts of Interest: The authors declare no conflict of interest.

References

1. Defraeye, T.; Blocken, B.; Koninckx, E.; Hespel, P.; Carmeliet, J. Aerodynamic study of different cyclist positions: CFD analysis and full-scale wind-tunnel tests. *J. Biomech.* **2010**, *43*, 1262–1268.
2. Barry, N.; Burton, D.; Sheridan, J.; Thompson, M.; Brown, N. Aerodynamic drag interactions between cyclists in a team pursuit. *Sports Eng.* **2015**, *18*, 93–103.

3. Fitzgerald, S.; Kelso, R.; Grimshaw, P.; Warr, A. Measurement of the air velocity and turbulence in a simulated track cycling team pursuit race. *J. Wind. Eng. Ind. Aerodyn.* **2019**, *190*, 322–330.
4. Barry, N. Aerodynamic Interactions between Multiple Cyclists. Ph.D. Thesis, Monash University, Clayton, Australia, 2015.
5. Blocken, B.; Toparlar, Y.; Van Druenen, T.; Andrianne, T. Aerodynamic drag in cycling team time trials. *J. Wind. Eng. Ind. Aerodyn.* **2018**, *182*, 128–145.
6. Martin, J.C.; Davidson, C.J.; Pardyjak, E.R. Understanding Sprint-Cycling Performance: The Integration of Muscle Power, Resistance, and Modeling. *Int. J. Sports Physiol. Perform.* **2007**, *2*, 5–21.
7. Crouch, T.; Burton, D.; Brown, N.; Thompson, M.C.; Sheridan, J. Flow topology in the wake of a cyclist and its effect on aerodynamic drag. *J. Fluid Mech.* **2014**, *748*, 5–35.
8. Crouch, T.; Burton, D.; Thompson, M.C.; Brown, N.; Sheridan, J. Dynamic leg-motion and its effect on the aerodynamic performance of cyclists. *J. Fluids Struct.* **2016**, *65*, 121–137.
9. Griffith, M.D.; Crouch, T.; Thompson, M.C.; Burton, D.; Sheridan, J.; Brown, N. Computational Fluid Dynamics Study of the Effect of Leg Position on Cyclist Aerodynamic Drag. *J. Fluids Eng.* **2014**, *136*, 101105.
10. Bearman, P.; Morel, T. Effect of free stream turbulence on the flow around bluff bodies. *Prog. Aerosp. Sci.* **1983**, *20*, 97–123.